$$\text{Fe}-\text{O}-\text{H}^{(0)} \;+\; \text{M}^{2+} \Leftrightarrow \text{Fe}_2\text{O}_3(s) \quad \text{M}-\text{O}\!\!<^{H}_{H}(+) + \text{H}^+ + \text{H}_2\text{O}$$

$$\text{Fe}_2\text{O}_3(s) \quad \text{M}-\text{O}\!\!<^{H}_{H}(+) + \text{M}^{2+} + \text{H}_2\text{O} \Leftrightarrow \quad \begin{array}{c}\text{Fe}_2\text{O}_3(s)\\ \text{MO}(s)\end{array} \quad \text{M}-\text{O}\!\!<^{H}_{H}(+) + 2\,\text{H}^+$$

Pekka Stén, Eini Puhakka, Ermo Ikävalko,
Jarmo Lehikoinen, Markus Olin, Pekka Sirkiä,
Petri Kinnunen & Timo Laitinen

Adsorption studies on iron oxides with reference to the oxide films formed on material surfaces in nuclear power plants

VTT

Adsorption studies on iron oxides with reference to the oxide films formed on material surfaces in nuclear power plants

Pekka Stén, Eini Puhakka, Ermo Ikävalko, Jarmo Lehikoinen, Markus Olin, Pekka Sirkiä, Petri Kinnunen & Timo Laitinen

VTT Processes
VTT Industrial Systems

The author´s present contact address
Vaasa Polytechnic, Environmental Engineering, Wolffintie 30, 65200 Vaasa
tel. +358 6 326 3031, fax +358 6 326 3112

Abstract

The construction materials used in coolant systems in nuclear power plants become covered with oxide films as a result of exposure to the aqueous coolant. The present work belongs to a research program on the properties of such films and especially on the transport of inorganic species through the films. The focus is on the incorporation of the highly energetic long-lived cobalt isotope ^{60}Co in the films causing build-up of radiation fields in the out-of-core system.

The present report concentrates on experimental adsorption studies both in ambient conditions and in high-temperature (573 K and 507 K), high-pressure conditions closely resembling those prevailing in the cooling circuits of nuclear power plants. In addition to cobalt adsorption, adsorption of zinc and nickel were studied, as a novel method to decrease the activity incorporation due to ^{60}Co is injection of zinc into the primary coolant. Potentiometric acid-base titrations of hematite suspensions were conducted in the presence and absence of adsorbing metal cations (Zn^{2+}, Co^{2+}, Ni^{2+}). Qualitatively the effect of adsorbed metal cation is noticed as a shift in the potentiometric titration curve, at a given pH more base is consumed due to the metal adsorption.

Adsorption of inorganic solutes on oxide surfaces is nowadays most frequently modelled by employing the surface complexation approach, which was succesfully used also in this study to explain the results of the room-temperature experiments. However, it was found that a simple surface complexation model was not accurate enough to reproduce the high-temperature titration data in the presence of a metal cation. A reasonable fit of the high-temperature experimental data was obtained by extending the surface complexation model to take into account surface precipitation. The tentative equilibrium constants of the adsorption reactions, extracted by FITEQL version 4.0 modelling software, were used to calculate high-temperature adsorption edges. Although there seems to be practically no difference in the high-temperature adsorption affinities between zinc and cobalt, it is easy to understand that zinc can, however, be used to retard cobalt adsorption provided that zinc concentration in the solution is considerable higher than cobalt concentration.

Contents

1. Introduction

In the operation of water-cooled nuclear reactors, the increase of radioactivity in the out-of-core system, e.g. piping, is a serious problem. The radioactive contamination is mainly due to the highly energetic long-lived cobalt isotope ^{60}Co. The natural cobalt isotope, ^{59}Co, is introduced in nuclear reactors both as an impurity of constituent steels and as major constituent of special alloys such as Stellite. The interaction between the construction materials and the aqueous coolant leads to the formation of oxide films on the piping surfaces and to the release of small amounts of metals, e.g. ^{59}Co, into the coolant. The released cobalt is carried by this coolant into the core of the nuclear reactor where the ^{60}Co isotope is formed by neutron activation of the natural cobalt. Finally, these activated species are redistributed in the cooling circuit and, subsequently, deposited on the system surfaces which are exposed to reactor water. This activity transport and the build-up of radiation fields may result in increased occupational doses of radiation for the personnel of the plant. A novel method to decrease the activity incorporation is injection of zinc into the primary coolant, although the exact mechanisms by which zinc affects are not known.

The incorporation of activated ^{60}Co species in the oxide films formed on material surfaces in the primary circuits in nuclear power plants is a complicated process, involving several steps. The phenomena taking place inside the oxide film have been thoroughly studied at VTT Industrial Systems employing sophisticated electrochemical techniques. In the work carried out at VTT Processes adsorption is assumed to be the first step of competitive interaction of various dissolved ions with the oxide film.

1.1 Surface complexation

In the adsorption studies, we adopt the surface complexation approach to elucidate the effects that solution conditions have on adsorption. This approach provides a thermodynamically consistent framework for modelling the distribution of solutes between aqueous solution and oxide surfaces and supplies a quantifiable basis for assessing the identity of those surface species that may act as precursors in further surface-controlled processes. The main concepts and various implementations of the surface complexation models were reviewed in our previous report (Stén et al. 2000). Suffice it to note here that applying the surface complexation approach, adsorption equilibria are considered as complexation reactions of the cations (e.g. cobalt and zinc) with surface hydroxyl groups ($\equiv$Fe–OH) which are formed on the mineral surface during its contact with the aqueous solution. These surface groups can adsorb protons or hydroxide ions as illustrated by reactions (1) and (2) as well as take part in complexation with metal ions, e.g. by the simplified reactions (3) and (4).

$$\equiv \text{Fe–OH} + \text{H}^+ = \equiv \text{Fe–OH}_2^+ \tag{1}$$

$$\equiv \text{Fe–OH} = \equiv \text{Fe–O}^- + \text{H}^+ \tag{2}$$

$$\equiv \text{FeOH} + \text{Co}^{2+} = \equiv \text{FeOCo}^+ + \text{H}^+ \tag{3}$$

$$\equiv \text{FeOH} + \text{Zn}^{2+} = \equiv \text{FeOZn}^+ + \text{H}^+ \tag{4}$$

Provided that adsorption reactions similar to (1)–(4) are quantified by means of equilibrium constants, the distribution of adsorbing species in the solution and on the surface can be calculated in various solution conditions. In our previous report (Stén et al. 2000) simplified adsorption calculations performed using the HYDRAQL modelling software were presented. In these calculations we relied on the thermodynamic data (valid at 25 $^\text{o}$C) compiled by Dzombak and Morel (1990), adopted their surface complexation model, the generalized two-layer model, and used one specific iron oxide, ferrihydrite (known also as hydrous ferric oxide), as the model sorbent. The calculations revealed that the experimentally observed retarding effect of zinc addition on cobalt incorporation can be quantitatively understood by means of competitive surface complexation.

1.2 Adsorption studies

The present report concentrates on experimental adsorption studies both in ambient conditions and in high-temperature high-pressure conditions. Although the main interest is on the high-temperature high-pressure adsorption, a few experiments in ambient conditions were performed in order to test the experimental approach and compare the obtained results with those published in the literature. Potentiometric acid-base titrations were conducted in the presence and absence of adsorbing metal cations. The experimental data was fitted into various adsorption models using the FITEQL version 4.0 modelling software in order to extract surface complexation constants of adsorption reactions similar to (1)–(4). The formulation of the equilibrium problem and the fitting procedure employing the FITEQL software are described in detail in our previous report (Stén et al. 2000). Qualitatively, the effect of adsorbed metal cation is noticed as a shift in the potentiometric titration curve, at a given pH more base is consumed due to the metal adsorption. Due to these shifts, the adsorption affinities of various metal ions can be qualitatively compared even in such cases where the quantitative parameter extraction procedure (model fitting) turns out to be mathematically unsuccessful.

2. Experiments at room tempereture

2.1 Titrations of hematite suspensions in the absence of adsorbing metals

The experimental work was started with acid-base titrations of hematite suspensions in an inert electrolyte. In this case, only reactions (1) and (2) need to be considered. Although the main interest in this project is the adsorption of metal ions on iron oxides and not the adsorption of H^+ and OH^- ions described by reactions (1) and (2), we decided to start with the simplest system for two reasons. Firstly, the chemistry of this system is as uncomplicated as it can be, and the chemically simple system is the best alternative for testing the experimental setup. Especially in the case of the high-temperature titrations, considerable effort was put on the development of the experimental system. Secondly, this system also comprises a subset in any study dealing with adsorption of aqueous species on iron oxide surfaces.

2.1.1 Experimental

Three commercial hematites, produced by Merck, Baker, and BDH, were examined and the BDH hematite was chosen for the first titration studies. It consisted of particles with an average size of 10 μm as well as of fine particles (< 1 μm), and the specific surface area determined by BET(N_2) was 2.5 m^2/g. The hematite structure was confirmed by XRD, and XRF did not show any impurities.

The titrations were conducted using suspensions containing 10 g of hematite in 100 ml of 0.1 M NaCl solution in a closed reaction vessel from which CO_2 (g) was excluded by nitrogen purge. Diluted acid or base (0.1 or 0.05 M NaOH or HCl solutions) was added at 0.05–0.1 ml increments from an automatic burette (Metrohm Titrino) to the suspension and after an equilibrium time of five minutes the electromotive force (emf) of a glass electrode–reference electrode cell was automatically registered. Assuming the absence of interfering ions and the activity coefficients to be constant, this emf at 298.15 K is given by

$$E_H = E_{o,H} + 59.157 \text{ mV} \log[H^+] + E_j \quad (5)$$

Here, $E_{o,H}$ is the apparatus constant and E_j is the liquid junction potential depending on ionic strength and free hydrogen ion concentration. Although there exist analytical expressions for the junction potential (e.g. Sjöberg et al. 1983), in the pH range of this work, the varying junction potential, however, has a minor influence compared to other sources of uncertainty. Consequently, E_j is approximated to be constant and included in

the $E_{o,H}$ term as is done for the activity coefficient which is assumed to remain constant throughout the titration. A schematic drawing of the room-temperature experimental setup is shown in Figure 1. Before starting the titration, the suspension was rinsed in the titration vessel with deaerated 0.1 M NaCl solution in order to remove adsorbed impurities. The rinsing was done in five steps, changing 50 ml of the solution in each step. After rinsing, a known excess of HCl, H_{added}, was added before starting the titration with 0.1 M NaOH solution. After completing the forward titration, back titration (decreasing pH) adding 0.05 M HCl was conducted with the same suspension.
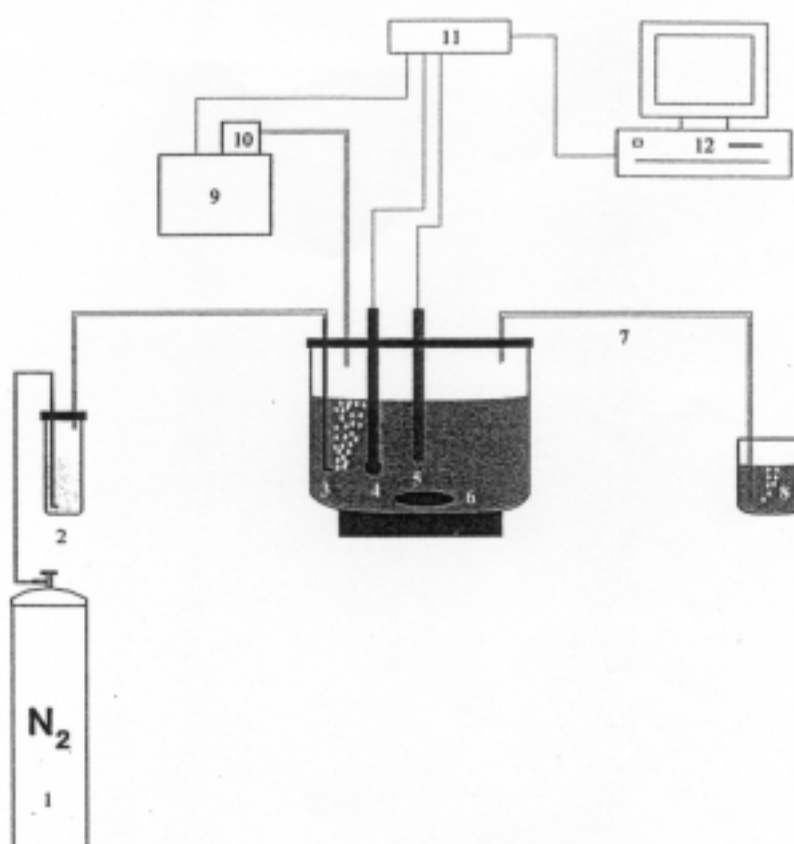

Figure 1. A schematic drawing of the room-temperature experimental set-up. 1: nitrogen cylinder, 2: background electrolyte, 3: nitrogen inlet, 4: glass electrode, 5: reference electrode, 6: magnetic stirrer, 7 and 8: nitrogen outlet, 9: autoburette, 10: deaerated titrant (0.1 M NaOH), 11: potentiometer, 12: computer.

2.1.2 Graphical evaluation of the titration results

2.1.2.1 Gran analysis

The first part of the forward titration can be used to determine the total amount of surface sites (more exactly, proton binding sites) on hematite. In the acidic pH range, the surface is saturated with protons and there is an excess of free hydrogen ions in the solution, H_o. In this acidic pH region, the titration is a strong acid-strong base titration, and by employing Gran's method (Gran 1952) it is possible to perform an accurate determination of excess protons, H_o, which is used to calculate the amount of adsorbed protons, H_s, as the difference

$$H_s = H_{added} - H_o \tag{6}$$

The free proton concentration during the first part of the titration can be expressed as

$$[H^+] = (H_o - V_t c_t) / (V_t + V_{beg}) \tag{7}$$

where V_{beg} is the volume of the titrated suspension in the beginning of the titration

V_t is the added volume of the titrant

H_o is the amount of excess protons in the beginning of the titration

c_t is the concentration of the titrant (NaOH)

Combining this equation with equation (5), gives

$$E_H = E_{o,H} + E_j + (0.059157 \text{ V})\log\left(\frac{H_o - V_t c_t}{V_{beg} + V_t}\right) \tag{8}$$

which can be further written in the forms

$$10^{\frac{E_H}{0.059157 \text{V}}} = 10^{\frac{E_{oH} + E_j}{0.059157 \text{V}}}\left(\frac{H_o - V_t c_t}{V_{beg} + V_t}\right) \tag{9}$$

$$(V_{beg} + V_t)10^{\frac{E_H}{0.059157 \text{V}}} = 10^{\frac{E_{oH} + E_j}{0.059157 \text{V}}}(V_{ef} - V_t)c_t \tag{10}$$

where V_{ef} is the equivalence volume of the titrant defined as $H_o = V_{ef}c_t$.

When the left-hand side of equation (9) (the Gran function) is plotted as a function of V_t, a straight line intercepting the V_t axis at V_{ef} is obtained, as shown in Figure 2. Actually, the linearity of the plot indicates that there is an excess of free hydrogen ions in this pH region. Further, the glass electrode can be calibrated *in situ* on a concentration scale employing the data observed in this acidic region. The sum, $E_{o,H} + E_j$, can be obtained

9

from the slope of the Gran plot. Due to this calibration procedure, $-\log[H^+]$ would be a more correct notation than pH in this report.
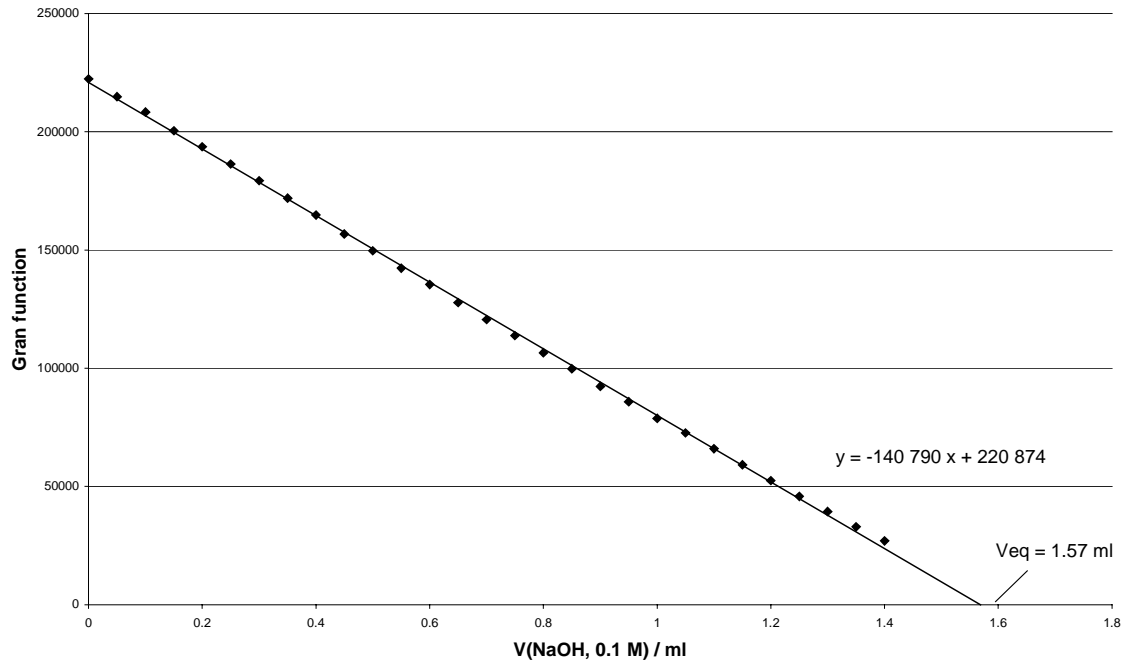

Figure 2. Gran plot analysis to determine the excess acid in solution and, consequently, the amount of adsorbed protons and the density of surface sites.

In the case illustrated in Figure 2, $0.2 \cdot 10^{-3}$ mol of HCl was added to the suspension. The Gran plot indicates that 1.57 ml of 0.1 M NaOH solution was needed to neutralize the excess acid in the solution. Hence, $0.043 \cdot 10^{-3}$ mol of protons were adsorbed on the surface, implying a surface site density of $1.7 \cdot 10^{-6}$ mol/m^2, which is somewhat lower than the value of $4 \cdot 10^{-6}$ mol/m^2 reported by Karasyova et al. (1999). A value of 364 mV is obtained for the sum, $E_{o,H} + E_j$, from equation (11)

$$-140790 = -c_t 10^{\frac{E_{oH} + E_j}{0.059157 V}}$$
(11)

2.1.2.2 Titration curves

A straightforward way to visualize the titration is to plot the pH as a function of the volume of added acid or base, as is done in Figure 3. As is mentioned above, the suspension was acidified by a known addition of HCl prior to starting the titration with NaOH. Hence, negative NaOH volumes on the *x*-axis of Figure 3 correspond to net addition of acid. The filled symbols represent the experimental forward (increasing pH) titration with NaOH, while the open symbols represent the consecutive experimental

back titration (decreasing pH) with HCl. A clear hysteresis is obtained indicating that reactions (1) and (2) are not totally reversible. The protons adsorbed in the initial acidification stage are not totally desorbed (reverse of reaction (1) and reaction (2)) during the forward titration with NaOH. Such hysteresis phenomena are well known and considered as a general feature of adsorption reactions. For comparison, a blank titration of HCl in the electrolyte is also illustrated in Figure 3 with the + symbols. The steep slope of the blank titration curve in the neutral region indicates no buffer capacity in contrast to the more gradual slopes of the curves illustrating the titrations of the suspension and showing considerable buffer capacity.
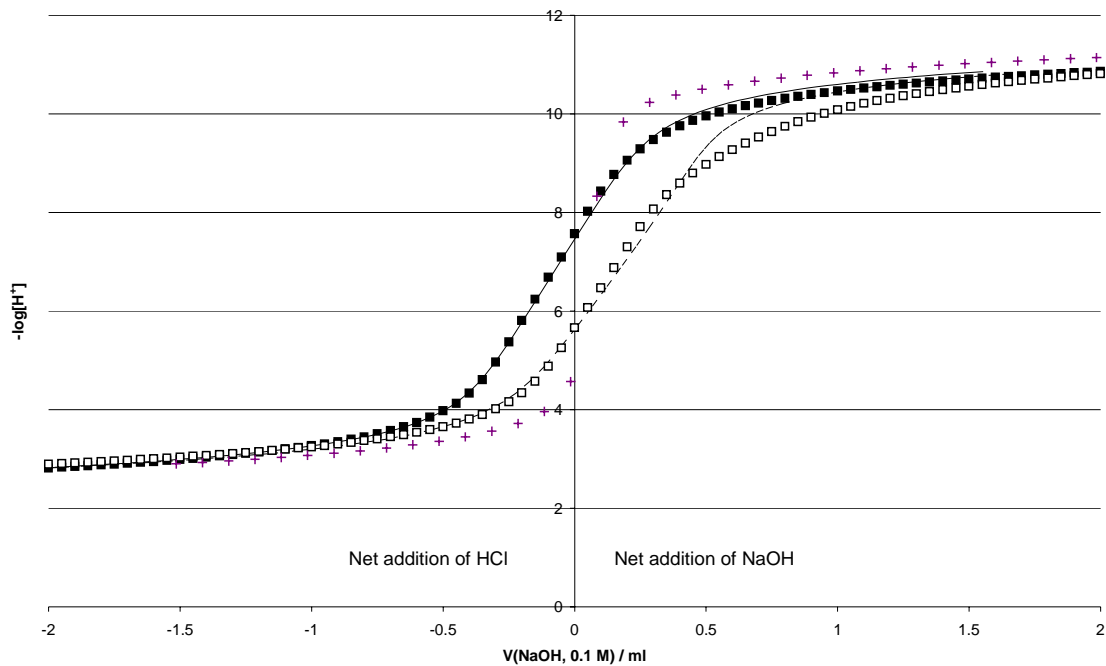

Figure 3. Titration curves of hematite suspension. Filled symbols and continuous line represent the forward titration (increasing pH) while open symbols and dashed line represent the back titration (decreasing pH). A titration curve of the mere electrolyte, i.e. blank (+), is given for reference. The procedure for obtaining the fitted curves is discussed below.

2.1.3 Fitting the experimental data to a reaction model

The lines shown in Figure 3 are simulated titration curves based on the constant capacitance model and the reactions given in Table 1. The values of the equilibrium constants presented in Table 1 are obtained by fitting the experimental titration data to the presented reaction model and dealing the electrical double layer according either to the constant capacitance model or the diffuse layer model. The constant capacitance and diffuse layer models, as well as the fitting procedure employing the FITEQL software,

are discussed in detail in our previous report (Stén et al. 2000). Suffice it to say here that the constant capacitance model and diffuse layer model are simple two-layer models describing the electrostatic aspects of the solid–solution interface. These models differ from each other only in the way of treating the completely hydrated non-specifically adsorbed counter-ions that balance out the charge resulting from the formation of the surface complexes, $\equiv Fe–OH_2^+$ and $\equiv Fe–O^-$ (in the present case). This difference is manifested in the different expressions for the interfacial capacitance. In the constant capacitance model, the interfacial capacitance is an adjustable parameter, while in the diffuse layer model the capacitance of the interfacial region is taken to be equal to the diffuse layer capacitance for which a theoretical expression is used.

Table 1. The reaction model used to fit the experimental titration data. The equilibrium constants of the surface reactions are the result of the optimization procedure.

Reaction	Logarithm of equilibrium constant	
	Constant capacitance model	Diffuse layer model
$\equiv Fe–OH + H^+ = \equiv Fe–OH_2^+$	6.87 (forward titration) 5.32 (back titration)	7.12 (forward titration)
$\equiv Fe–OH = \equiv Fe–O^- + H^+$	−8.06 (forward titration) −5.90 (back titration)	−7.82 (forward titration)
$H_2O = H^+ + OH^-$	−13.8 (ion product of water at 0.1 M ionic strength, Sjöberg et al. 1983)	

While employing the constant capacitance model, the value, 1.10 F/m^2, was taken for the specific capacitance (Karasyova et al. 1999) without further optimization. Both of the studied models explain the experimental titration data equally well, which is shown by the WSOS/DF values given by FITEQL; 30 (for the diffuse layer model) and 36 (for the constant capacitance model). WSOS/DF in the FITEQL output means the weighed sum of squares of residuals divided by the degrees of freedom, i.e. the overall variance, and is the main indicator of the goodness of fit. The constant capacitance model was used also in a tentative fitting of the back titration data. Due to the clear hysteresis, it is not surprising that the fitted equilibrium constants differ from those obtained by fitting the forward titration data. As can be seen from Figure 3, the model does not explain well the back titration data, which is illustrated also by the high value of WSOS/DF, 102.

2.2 Titrations of hematite suspensions in the presence of cobalt

2.2.1 Titration curves

Figure 4 illustrates the effect of adsorbed cation on the alkalimetric titration curve of hematite suspension. Three titration curves are shown. Curve A is given for reference and visualizes a titration of an acidified hematite suspension without any added cobalt. In the two other titrations, B and C, visualized in Figure 4, $CoCl_2$ solution was added to a neutral hematite suspension after rinsing but prior to performing an alkalimetric titration with 0.1 M NaOH. The amount of added cobalt (10 μmol in titration B and 30 μmol in titration C) corresponds to 20% or 60% of the surface sites ($\equiv$Fe–OH) available. As can be seen in Figure 4, in the presence of Co^{2+}, the titration curves are shifted in the expected way, at a given pH more base is consumed, and the shift depends on the amount of added cobalt. Most of the adsorption reactions of cations (e.g. 3) imply simultaneous release of protons leading to such shifts of the titration curves.
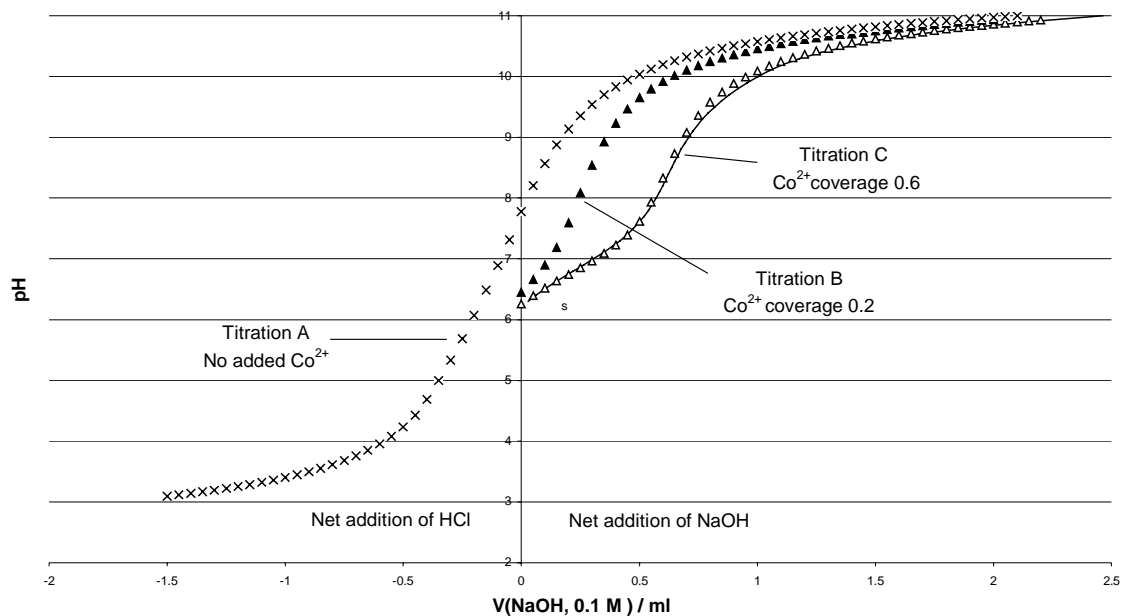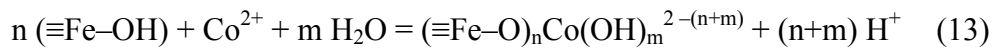

Figure 4. Shift of the alkalimetric titration curve of a hematite suspension due to the addition of adsorbing Co^{2+}. Titration A is conducted in the absence of cobalt, while in titrations B and C cobalt additions corresponding to 20% and 60% of the surface sites, respectively, are done. The solid line is a simulated titration curve based on the reaction model presented in Table 2.

13

2.2.2 Model fitting

Provided that equilibrium constants for the relevant solution reactions and the H^+ and OH^- adsorption reactions (1) and (2) are known, the shifted titration curve can be used to determine equilibrium constants for the Co^{2+} adsorption reactions. Generally, this information is supplemented by taking aliquots of the suspension and analysing the adsorbing metal in the aqueous phase, which helps to identify the number and stoichiometry of the adsorption reactions needed to adequately quantify the experimental data. However, even in the absence of such supplementary information, various plausible reaction models can be tried and the one giving the best fit is chosen to describe the adsorption system.

The diffuse layer model and two adsorption reactions, (12) and a reaction of the general form (13), were tried to fit the experimental data of titration C shown in Figure 4.

$$\equiv Fe–OH + Co^{2+} = \equiv Fe–OHCo^{2+} \qquad (12)$$

$$n\,(\equiv Fe–OH) + Co^{2+} + m\,H_2O = (\equiv Fe–O)_n Co(OH)_m^{2-(n+m)} + (n+m)\,H^+ \quad (13)$$

where $n = 1$ or 2 and $m \geq 0$.

An excellent fit was found for $n = 2$ and $m = 3$ as is evident by comparing the experimental data in Figure 4 with the simulated titration curve. A low value of 2.5 for the indicator of goodness of fit (WSOS/DF) given by FITEQL further confirms the excellent fit. As shown in Table 2, four known solution hydrolysis reactions of cobalt were also taken into account and the H^+ and OH^- adsorption reactions were described by equilibrium constants optimized from the acid-base titrations conducted in the absence of adsorbing metals. The surface species considered in the model and presented in Table 2 are schematically illustrated in Figure 5.

Table 2. The reaction model used to explain the alkalimetric titration data in the presence of added cobalt.

| Reaction	Logarithm of equilibrium constant	Reference
$H_2O = H^+ + OH^-$	-13.8	Sjöberg et al. 1983
$Co^{2+} + H_2O = Co(OH)^+ + H^+$	-9.65	Baes and Mesmer 1976
$Co^{2+} + 2\ H_2O = Co(OH)_2 + 2\ H^+$	-18.80	Baes and Mesmer 1976
$Co^{2+} + 3\ H_2O = Co(OH)_3^- + 3\ H^+$	-31.50	Baes and Mesmer 1976
$Co^{2+} + 4\ H_2O = Co(OH)_4^{2-} + 4\ H^+$	-45.78	Smith and Martell 1976
$\equiv Fe-OH + H^+ = \equiv Fe-OH_2^+$	7.35	this work (no cobalt)
$\equiv Fe-OH = \equiv Fe-O^- + H^+$	-7.75	this work (no cobalt)
$\equiv Fe-OH + Co^{2+} = \equiv Fe-OHCo^{2+}$	6.54	this work (titration C)
$2\ (\equiv Fe-OH) + Co^{2+} + 3\ H_2O = (\equiv Fe-O)_2Co(OH)_3^{3-} + 5\ H^+$	-29.51	this work (titration C)
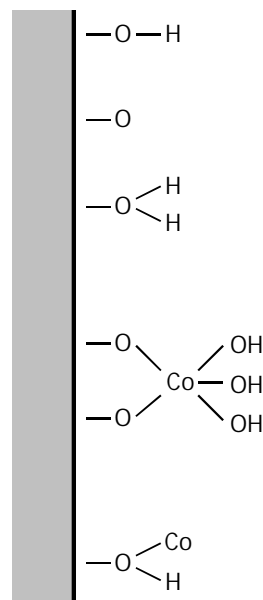
Figure 5. A schematic illustration of the surface species used to explain cobalt adsorption on hematite employing the double layer model.

Titration curve shifts are seldom used to measure adsorption, but the classical approach in adsorption studies is the wet chemical batch measurement of the extent to which the adsorbent (solid) removes the adsorbate (dissolved metal) from a solution. Adsorption of metals is usually strongly dependent on pH and, consequently, the adsorption data obtained at constant sorbate and sorbent concentrations are commonly presented in plots of percent sorbed versus pH, referred to as pH edges. Increasing uptake with increasing pH until a plateau at 100% is reached is typical of cation adsorption on metal oxides. Typically, adsorption increases from hardly measurable values to almost 100% of the amount added over a narrow region of 1–2 pH units, termed the adsorption edge. Provided that the experimental titration data in the presence of an adsorbing metal have been succesfully fitted to a plausible reaction model (as shown in Figure 4), this model can be used to calculate a simulated pH edge, as is done in Figure 6.
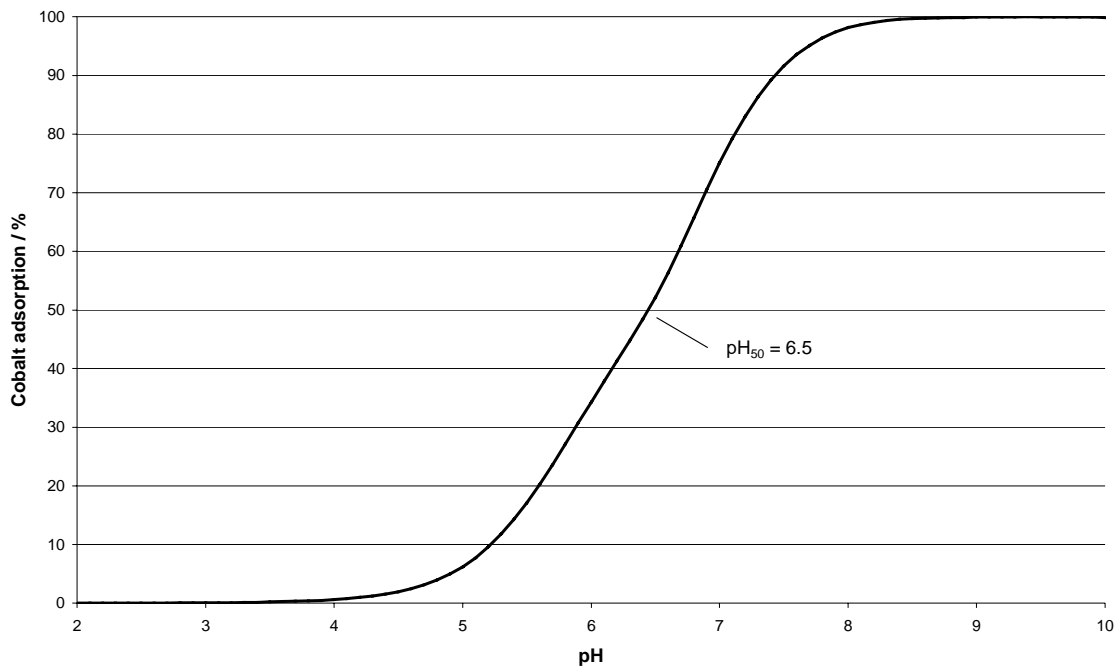

Figure 6. Cobalt adsorption on hematite at room temperature. A simulated pH edge based on the reaction model presented in Table 2. 50% of the added cobalt is adsorbed at pH 6.5 as indicated on the curve.

3. Experiments at high temperature and pressure

Several titrations were conducted in order to study the acid-base and adsorption properties of hematite suspensions in conditions closely resembling those prevailing in the cooling circuits of nuclear power plants. Three tasks for these studies can be defined: 1) testing the suitability of the available apparatus for high-temperature adsorption studies, 2) comparing qualitatively the adsorption affinities of zinc, cobalt, and nickel, and 3) collecting data for extraction of parameters to be used in quantitative adsorption modelling at high temperature. Two experimental campaigns employing two different autoclaves were conducted. The first campaign was conducted in a nickel autoclave and concentrated on zinc adsorption and acid–base properties of hematite at 300 ^{o}C. The second campaign was conducted in a teflon-lined autoclave at 234 ^{o}C, and along with acid-base properties of hematite, adsorption of zinc, cobalt, and nickel was studied.

3.1 Titrations in a nickel autoclave

3.1.1 Experimental

The first high-temperature titrations were conducted in a four-liter nickel autoclave specially designed at VTT Industrial Systems and extensively used to simulate the power plant conditions. The 0.1 M NaOH titrant was manually dosed by a high-pressure chromatography pump having a constant flow rate of 2 ml/min. Mixing of the hematite suspension during the titration was realized by bubbling the nitrogen (AGA 5.0) used for the pressure adjustment through a perforated metal spiral installed at the bottom of the autoclave. The pH was measured with an oxygen-ion-conducting ceramic membrane sensor based on yttrium stabilized zirconium oxide, ZrO_2 (Y_2O_3), and a NiO/Ni internal reference couple. A silver–silver chloride electrode filled with 0.005 M KCl was used as the reference electrode. A platinum wire was available for the redox measurement and the potential values were registered manually with commercial multi-meters. The sensors employed in the measurements are specially designed and manufactured at VTT Industrial Systems as one of the results of a long-standing development work on techniques for electrochemical studies in power plant environments. A summary of this sensor development work is given by Mäkelä (2000) and a detailed description of the employed specific measurement system by Macdonald et al. (1992).

The titrations were started by adding 4 liters of 0.1 M $NaNO_3$ background electrolyte in the autoclave. Dissolved carbon dioxide was removed from the electrolyte by gently warming and bubbling nitrogen through it during one hour prior to the addition of 400 g of hematite (BDH). The solid–solution ratio was the same as in the room-temperature

17

titrations and the amount of surface sites was estimated to be 2 mmol based on the room-temperature measurements (specific surface area 2.5 m^2/g and surface site density 2 μmol/m^2). To remove adsorbed impurities, the suspension was rinsed with deaerated electrolyte. The rinsing was done in three steps, changing ca. 1500 ml of the electrolyte in each step. The rinsing procedure conducted in a closed and gently warmed (ca. 60 ^{o}C) autoclave was as follows: a) by using a T-valve the nitrogen flow mixing the suspension was moved on top of the solution and the suspension was allowed to settle for 30 min, b) the autoclave was gently pressurized and 1500 ml of clear electrolyte was tapped out through an outlet dipping in the bulk of the solution, c) after adding a new aliquot of electrolyte, the suspension was mixed by leading nitrogen through it for ca. 10 minutes. Followed by the last aliquot of deaerated rinsing solution, a known amount of nitric acid (typically 6 ml of 1.0 M solution) was added to saturate the hematite surfaces with protons. In the two experiments on zinc adsorption, zinc nitrate (8 ml and 16 ml of 0.1 M solution) was added at this stage, after which the autoclave was warmed up to 300 ^{o}C, taking about 2–3 hours. During warming the suspension was mixed by nitrogen flow, the pressure was gradually increased and adjusted to 120 bars at the final temperature. In the titrations, 2 ml aliquots of the titrant (0.1 M NaOH) were dosed by manually operating the pump for one minute, after which an equilibration time of two minutes was allowed before measuring the potentials a) between the pH electrode and the autoclave body, b) between the reference electrode and the autoclave body, and c) between the platinum wire dipping in the suspension and the autoclave body. A full titration took typically about two hours.

3.1.2 Results

3.1.2.1 Titration curves

Three titration curves obtained at 300 ^{o}C in the nickel autoclave are shown in Figure 7. The pH values given on the *y*-axis are obtained by strictly thermodynamic means from the measured potential values, as discussed by Macdonald et al. (1992). As mentioned above, all the suspensions were acidified by adding 6 ml of 1 M HNO_3 prior to starting the titration with 0.1 M NaOH. Hence, negative NaOH volumes on the *x*-axis of Figure 7 correspond to net addition of acid, expressed as the added volume of virtual 0.1 M acid. In titration D, no zinc is added, while in the other titrations, in addition to nitric acid, zinc nitrate additions corresponding to 40% (0.8 mmol Zn^{2+}, curve E) and 80% (1.6 mmol Zn^{2+}, curve F) of the available hematite surface sites are made. As mentioned above, the amount of hematite surface sites, 2 mmol, is based on the measurements at room temperature.
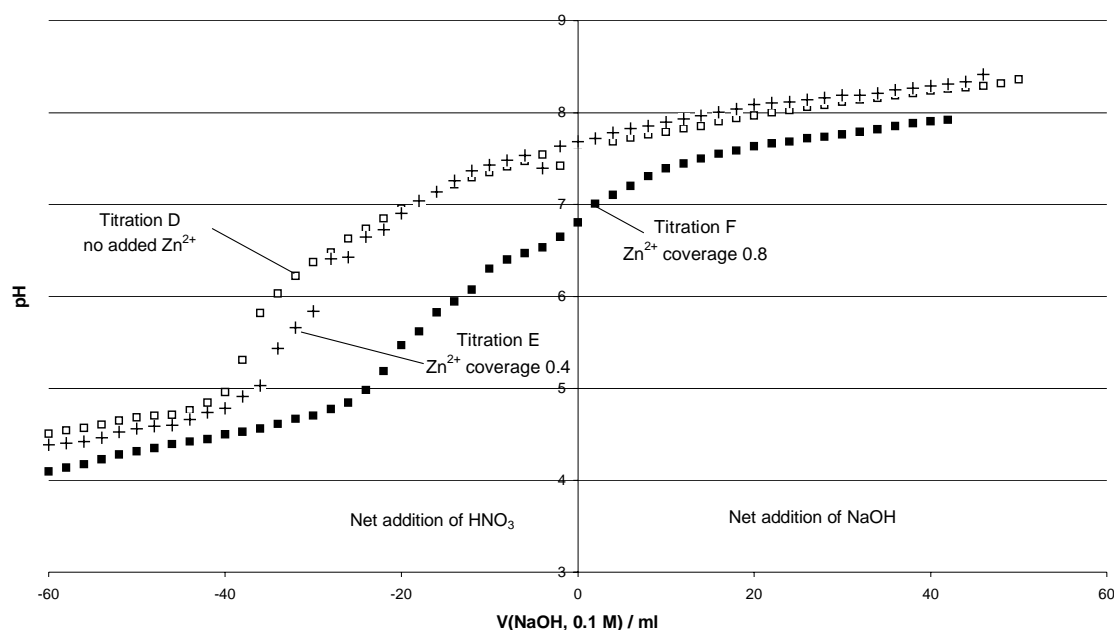
Figure 7. Shift of the high-temperature (300 ^{o}C, Ni autoclave) titration curve of a hematite suspension due to the addition of adsorbing Zn^{2+}. Titration D (open symbols) is conducted in the absence of zinc, while in titrations E (+) and F (filled symbols) zinc additions corresponding to 40% and 80% of the surface sites, respectively, are done.

Although the shape of the titration curves is not as good as in the room-temperature titrations (cf. Figure 4), the effect of added zinc is clearly seen. The titration curves are shifted in the expected way, at a given pH more base is consumed, and the shift depends on the amount of added zinc. An obvious difference to the room temperature titration curves is the location of the pH break. When comparing curve D with curve A (in Figure 4), we note that at high temperature the steep increase in pH takes place earlier in the course of the titration, at a stage where the amount of added NaOH is far less than equivalent to the amount of acid added in the initial acidification step. This indicates that the acid is partly consumed by some non-reversible process, e.g. dissolution of hematite or nickel, or both.

3.1.2.2 Analyses

After finishing titrations D, E, and F, clear samples were taken from the settled and cooled-down suspension for Fe, Ni and Zn analyses with AAS. The results of these analyses are given in Table 3, which also contains analysis results after finishing two other titrations, AB1 and AB2. AB1 and AB2 were initial tests, in which 5 ml of 1 M HNO_3 was diluted in four liters of the background electrolyte and titrated at 300 ^{o}C with 0.1 M NaOH.

Table 3. AAS analysis results of solution samples taken at high pH from the cooled-down and settled suspensions after finishing the titrations.

Titration	Analyzed concentrations / 10^{-6} mol dm^{-3}		
	Fe	Ni	Zn
D	0.48	0.13	not analyzed
E	0.47	0.16	0.84
F	0.59	0.12	0.74
AB1, HNO$_3$–NaOH	3.6	2.9	not analyzed
AB2, HNO$_3$–NaOH	1.6	0.27	not analyzed

All the analyzed concentrations are low compared to the concentration of hematite surface sites ($5 \cdot 10^{-4}$ M), the analyzed zinc concentrations correspond to 0.4% (E) and 0.2% (F) of the zinc added, and the concentrations in the test titrations are higher than the concentrations in titrations containing hematite. As the samples were taken at high pH after finishing the titrations, low dissolved metal concentrations are rather expected. However, the higher Ni concentrations in the test titrations conducted in the absence of any suspension indicate dissolution of nickel from the autoclave body and readsorption of this nickel on hematite. This is, indeed, confirmed by XRF analyses of the dried hematite powder before and after titration. In four untreated hematite samples, Ni concentrations were found to be between 0.002% and 0.006%, i.e. at the detection limit, while 0.03% Ni was found in the sample taken from the suspension after titration. Although XRF, especially at low concentrations, should be considered a semi-quantitative method, such an increase is significant, and the analyzed amount of Ni is of the same order of magnitude as the amount of surface sites. Hence, instead of studying zinc adsorption, we studied in these first high-temperature titrations the competitive adsorption of zinc and nickel. In contrast to XRF, XRD analysis did not reveal any changes due to the high temperature treatment.

3.2 Titrations in a teflon-lined autoclave

3.2.1 Experimental

To overcome the problems caused by nickel dissolving from the autoclave body, the second experimental campaign was conducted in a teflon-lined autoclave. A commercial 200 ml autoclave (Berghof BAR 945 with Berghof RHS 295 heater) equipped with a magnetic stirrer was employed. The 0.1 M NaOH titrant was dosed manually from a programmable Shimadzu LC-10AD high-pressure chromatography

pump. The pH was measured with specially designed sensors similar to those used in the nickel autoclave, for which purpose a new autoclave cover had to be designed and tooled at VTT Industrial Systems. Two reference electrodes had to be used in this campaign as the first one was broken during the experiments. Due to the limited thermal inertness of teflon and the power of the heater employed, the titrations were conducted at 234 ^{o}C and 40 bar. Nitrogen (AGA 5.0) was needed only for initial deaeration and pressure adjustment as the suspension was stirred with a magnet.

A suspension containing 10 g of hematite in 100 ml of 0.1 M $NaNO_3$ was rinsed prior to titrations with deaerated 0.1 M $NaNO_3$ in the same way as in the room-temperature titrations employing 50-ml volumetric pipettes. After rinsing, the suspension was acidified by adding 0.3 ml of 1 M HNO_3 and eventually also 0.25 ml of 0.1 M zinc, nickel or cobalt nitrate solution prior to pressurizing and warming up the autoclave. Based on measurements at room temperature, the amount of surface sites on hematite was $5 \cdot 10^{-5}$ mol, hence, such metal additions correspond to 50% surface coverages. In the titrations, 0.1 ml additions of 0.1 M NaOH solution were done by manually operating the NaOH pump with a constant flow rate (0.05 ml/min) for two minutes, and after an equilibration time of one minute, the potential between the pH and reference electrodes was measured with a commercial multi-meter.

3.2.2 Results

Five selected high-temperature titration curves are shown in Figure 8. In titrations G and L, no metals are added in the acidified hematite suspension, while in titrations H, J, and K, zinc, nickel, and cobalt additions, respectively, corresponding to half of the hematite surface sites, are made. Due to the metal additions, the titration curves are shifted in the expected way, as is clearly seen by comparing titration J with titration G, and titration H with titration L. As mentioned earlier, two reference electrodes had to be used during this experimental campaign. Although both reference electrodes were prepared in the same way as described by Mäkelä (2000), changing the reference electrode caused a potential shift of ca. 100 mV, as can be seen by comparing titrations J and G with titrations H and L. However, no explanation can be given for the fact that curve K deviates from curves L and H in the beginning (small V(NaOH) values) of the titrations.

The measured potential values between the reference and pH electrodes can be converted to pH either by strictly thermodynamic means (Macdonald et al. 1992, Mäkelä 2000) or by employing the Gran procedure for an operational in situ calibration of the pH electrode-reference electrode cell on a concentration scale. As Figure 8 indicates differences between the employed reference electrodes, we decided to use the

Gran procedure and titration L for calibrating the pH electrode-reference electrode 1 cell and titration G for calibrating the pH electrode-reference electrode 2 cell.
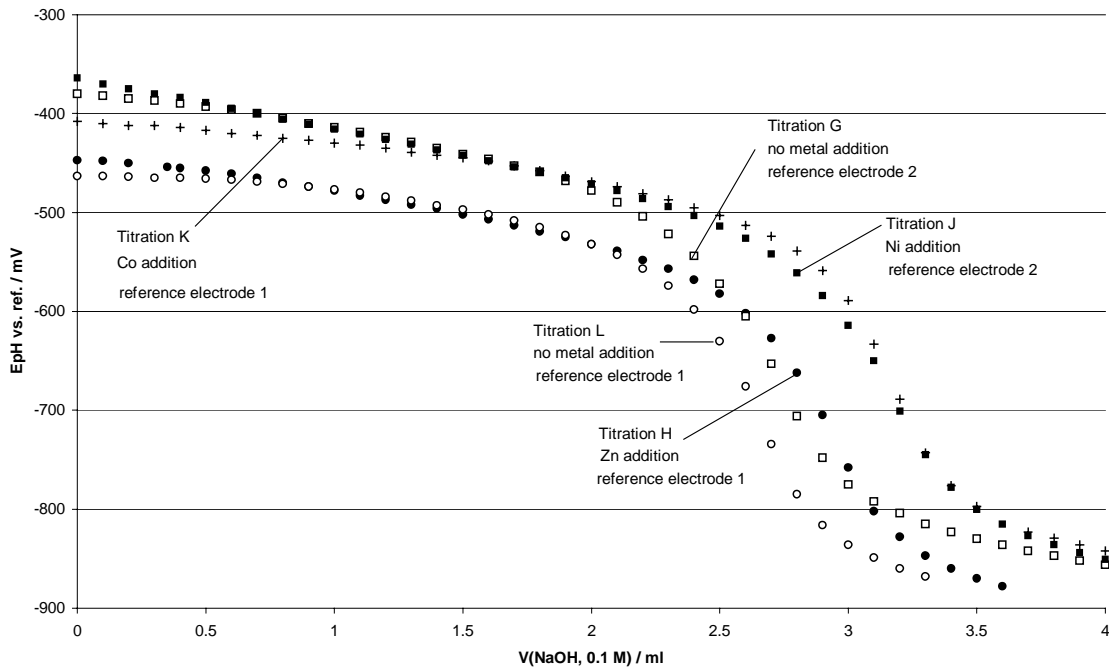

Figure 8. Measured potential values between the reference and pH electrodes during five high temperature titrations of acidified hematite suspensions. Titration G (open squares) and titration L (open circles) are conducted in the absence of added metals. Titration H (filled circles) is conducted in the presence of added zinc, titration J (filled squares) in the presence Ni, and titration K (+) in the presence of cobalt.

At 234 °C Equation (5) is written in the form

$$E_H = E_{o,H} + 100.61 \text{ mV} \log[H^+] + E_j \tag{14}$$

From the slope of the Gran plot (Figure 9) a value of −105 mV is determined for the term, $E_{o,H} + E_j$, according to equation (15) (which is analogous to equation 11)

$$-0.0090943 = -c_t 10^{\frac{E_{oH}+E_j}{0.10061V}} \tag{15}$$

Hence, the potential values measured against reference electrode 2 are converted to pH (on a concentration scale) acording to

$$-\log[H^+] = (-105 \text{ mV} - E_H)/100.61 \text{ mV} \tag{16}$$

resulting in the titration curves G an J in Figure 10. Although the Gran plot shown in Figure 9 is rather good, this procedure is not problem-free. The amount of surface sites

obtained from the V_{eq} value in Figure 9 is twice as high, $1 \cdot 10^{-4}$ mol, as the value based on room-temperature measurements. A more serious problem is that in this case the $E_{o,H} + E_j$ value obtained by the Gran calibration implies pH values one unit lower than those obtained by strictly thermodynamic means (Macdonald et al. 1992).
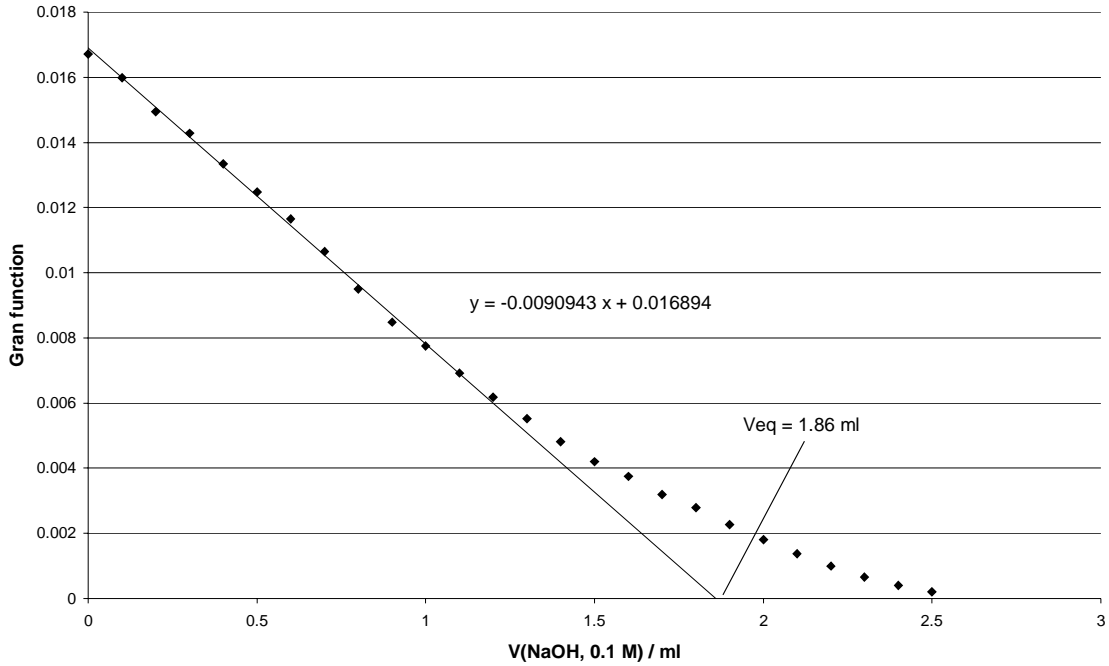

Figure 9. Gran plot of the titration of an acidified hematite suspension (titration G).

Applying the Gran procedure to titration L, a value of -188 mV is obtained for the term, $E_{o,H} + E_j$. Consequently, the potential values measured against reference electrode 1 are converted to pH (on a concentration scale) according to

$$-\log[H^+] = (-188 \text{ mV} - E_H)/100.61 \text{ mV} \tag{17}$$

resulting in the titration curves L, H, and K in Figure 10.

Although there is uncertainty in the measured potentials and especially in converting the potentials to pH values, Figure 10 supports the employed Gran procedure. The curves representing titrations L and G conducted with different reference electrodes are reasonably similar and all curves, except K, coincide at the acidic end of the titrations. Based on room-temperature experiments, it can be expected that at the acidic end of the titrations the added metals are not adsorbed. Consequently, the pH at the acidic end of the titration should not significantly depend on the properties of the added metal. Based on this assumption, in Figure 11 the experimental points representing titration K (in the presence of Co addition) are shifted 0.5 pH unit up to make all the titration curves

coincide at the acidic end of the titration. This shift corresponds to changing the $E_{o,H} + E_j$ value from –188 mV to –130 mV.
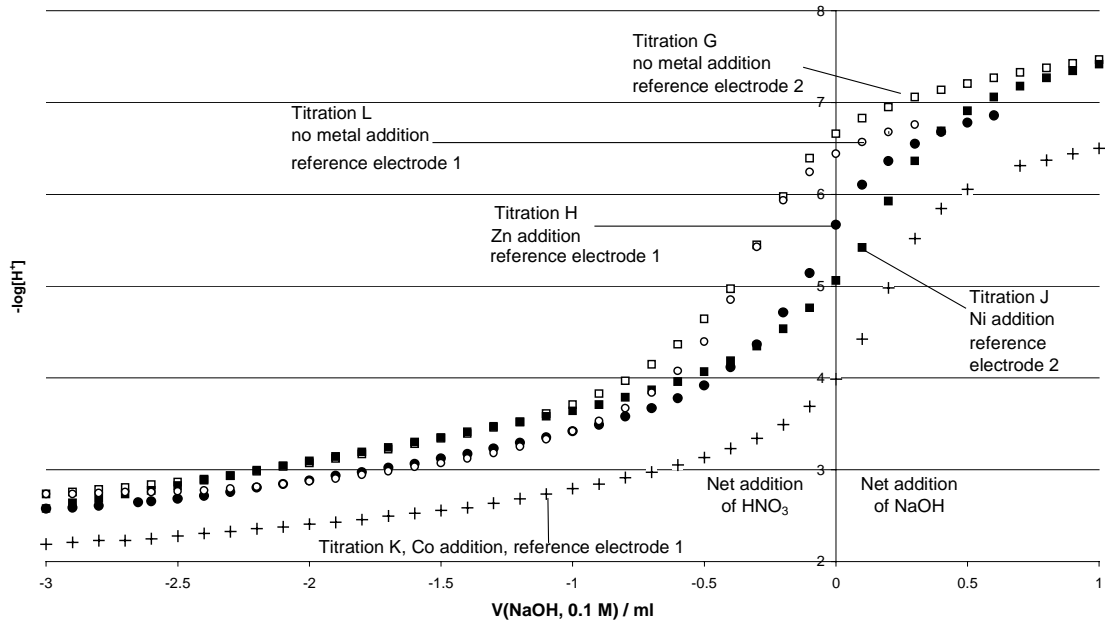

Figure 10. The data of Figure 10 presented as ordinary titration curves.
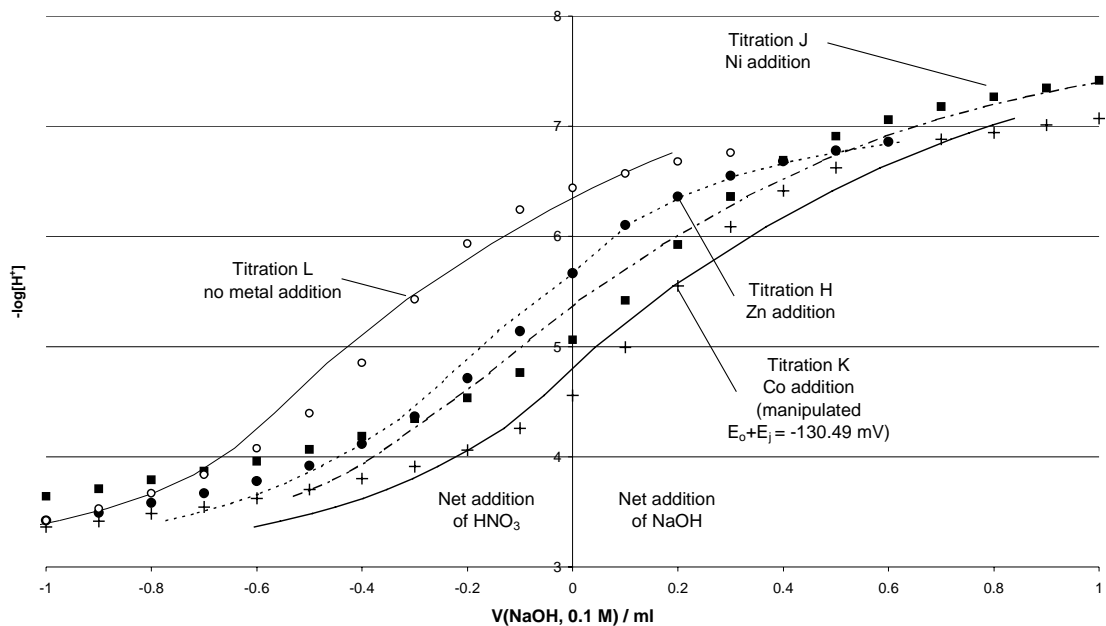

Figure 11. Experimental and simulated titration curves. The experimental points representing titration K (in the presence of Co addition) have been shifted 0.5 pH unit up to make all the titration curves coincide at the acidic end of the titration. The lines are simulated titration curves discussed below.

3.3 Model fitting

In spite of the uncertainties in the experimental [H^+] values, we employed FITEQL and the constant capacitance model in tentative fitting exercises of the high-temperature titration data. However, prior to any fitting, a minor modification of the FITEQL source code was found necessary. Based on the data of Fernández et al. (1997), a value of 31.5 was used for the static dielectric permittivity of water, ε, at 507 K. Yet, it was found that a simple surface complexation model was not accurate enough to reproduce the high-temperature titration data in the presence of a metal cation. For this reason, the surface precipitation model, proposed by Farley et al. (1985) and clearly summarized by Dzombak and Morel (1990), was tested to explain the measured high-temperature data.

3.3.1 Surface precipitation model

Surface precipitation model provides a construct for a continuum between surface complexation and bulk solid precipitation. It predicts the dominance of surface complexation at low surface coverages, while at higher surface coverages, the formation of a surface precipitate in the form of a solid solution begins to dominate the sorption process. In Figure 12, a schematic representation of the surface precipitation of a cation on hematite is depicted.
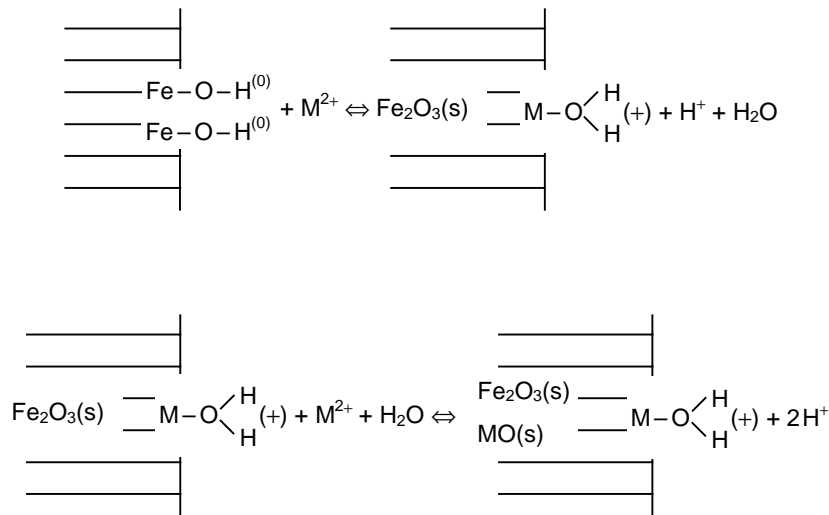

Figure 12. Schematic representation of the surface complexation and surface precipitation descriptions for sorption of a metal cation M^{2+} on hematite (modified from Dzombak and Morel (1990)). Formation of an oxide of the sorbing metal, MO(s), is shown as an example.

According to the surface precipitation model, adsorption of the cation on hematite is described as

$$2[(OH)_2 = Fe-OH] + M^{2+} = Fe_2O_3(s) + [OH-M-OH_2^+] + H^+ + H_2O \quad (18)$$
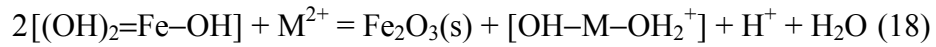
where brackets denote surface sites, which on hematite are formed according to

$$Fe_2O_3 + 3H_2O = 2[(OH)_2 = Fe-OH] \quad\quad\quad\quad\quad (19)$$
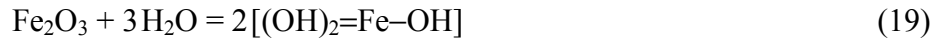
A more common convention is to simply write equation (18) as

$$2 \equiv FeOH^\circ + M^{2+} = Fe_2O_3(s) + {=}MOH_2^+ + H^+ + H_2O \quad\quad\quad (20)$$
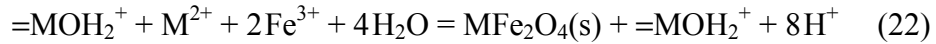
where $\equiv$ and $=$ denote bonds at the surface and have different meanings for Fe^{3+} and M^{2+}: $\equiv FeOH^\circ$ and $=MOH^\circ$ represent $[(OH)_2 = Fe-OH]$ and $[(OH)-M-OH]$, respectively.

At high concentrations, cations may sorb via precipitation as an oxide according to

$$=MOH_2^+ + M^{2+} + H_2O = MO(s) + {=}MOH_2^+ + 2H^+ \quad\quad\quad (21)$$
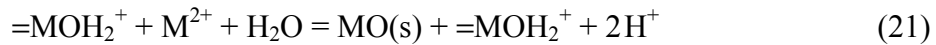
or as a ferrite according to

$$=MOH_2^+ + M^{2+} + 2Fe^{3+} + 4H_2O = MFe_2O_4(s) + {=}MOH_2^+ + 8H^+ \quad (22)$$

In the surface precipitation model, cations at the oxide–water interface are treated as surface species, while those not in contact with the solution phase are treated as solid species forming a solid solution. Along with the adsorption and precipitation of the sorbing cation, the solubility of the sorbent (hematite, in our case), is taken into account in the surface precipitation model according to

$$\equiv FeOH^\circ + 2Fe^{3+} + 3H_2O = Fe_2O_3(s) + {\equiv}FeOH^\circ + 6H^+ \quad\quad\quad (23)$$
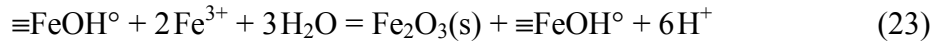
In the surface precipitation model, an additional parameter, $[Fe_2O_3]_T$, the initial amount of sorbent solid that can participate in the solid solution, must also be specified. This parameter is expected to be a small fraction of the total oxide solid concentration added to the system, accounting for the fact that only the surface and some of the first few layers of the sorbent will participate in the solid solution with the co-precipitating metal ion. The value chosen for this parameter depends on the particle size, shape, and morphology. Hence, it can be considered a fitting parameter. In the present calculations, the order of magnitude for $[Fe_2O_3]_T$ was found to be 10^{-4} mol/l. This means that only

about 0.02% of the hematite mass participates in the solid solution, thus supporting the surficial character of the phenomenon.

Due to the slow kinetics of metal diffusion into the hematite structure (Nishino et al. 1989), formation of stable oxide and ferrite phases on the surface was considered unlikely within the experimental time. Therefore, equations (21) and (22) were omitted from the final calculations and, consequently, the employed model should be considered as a semi-surface-precipitation model. Although there exists uncertainty also about the hematite dissolution–precipitation kinetics, equation (23) turned out to be decisive for a good fit, regardless of whether equations (21) and (22) were included or not.

3.3.2 Results and discussion

The reactions given in Table 4 were considered while modelling the titration data obtained in the absence of added metals (titration L). Along with equilibrium constants for the surface hydrolysis reactions given in Table 4, an optmized value of $6.0 \cdot 10^{-6}$ mol/g) was found for the surface site density. The capacitance was varied manually and the best fit illustrated in Figure 11 was obtained with a value of 2.6 F/m^2. Although the fit illustrated in Figure 11 is far from perfect and there is considerable uncertainty in the measured pH values, it is interesting to note that the experimental point of zero charge obtained as the mean of the pK_a values ($pK_{a1} = 6.1$, $pK_{a2} = 6.8$) is the same, ~6.6, as that estimated by Schoonen (1994).

Table 4. The reaction model used to fit the high-temperature titration data obtained in the absence of added metals (titration L).

Reaction	Logarithm of equilibrium constant	Reference
$H_2O = H^+ + OH^-$	−10.83	Marshall and Franck 1981
$\equiv Fe–OH + H^+ = \equiv Fe–OH_2^+$	6.1	optimized
$\equiv Fe–OH = \equiv Fe–O^- + H^+$	−6.8	optimized

In addition to the reactions presented in Table 4, the precipitation-dissolution equilibrium of hematite shown in Table 5 must be taken into account while employing the surface precipitation model. Further, by considering the known hydrolysis reactions according to Table 5, simulated titration curves in the presence of added metals were calculated and are shown in Figure 11.

Table 5. Additional reactions needed in the surface precipitation model to explain the data of titrations H, J and K.

	Logarithm of equilibrium constant[†]	Reference
$\equiv\!FeOH° + 2\,Fe^{3+} + 3\,H_2O =$ $Fe_2O_3(s) + \equiv\!FeOH° + 6\,H^+$	8.0	Wolery 1992
$Fe^{3+} + H_2O = Fe(OH)^{2+} + H^+$	–0.7	Ishigure et al. 1992
$Fe^{3+} + 2\,H_2O = Fe(OH)_2{}^+ + 2\,H^+$	–2.1	Ishigure et al. 1992
Titration H		
$2\!\equiv\!FeOH° + Zn^{2+} =$ $Fe_2O_3(s) + =\!ZnOH_2{}^+ + H^+ + H_2O$	–2.6	optimized
$Zn^{2+} + H_2O = Zn(OH)^+ + H^+$	–5.3	Bénézeth et al. 2002
$Zn^{2+} + 2\,H_2O = Zn(OH)_2 + 2\,H^+$	–10.9	Bénézeth et al. 2002
$Zn^{2+} + 3\,H_2O = Zn(OH)_3{}^- + 3\,H^+$	–18.9	Bénézeth et al. 2002
Titration J		
$2\!\equiv\!FeOH° + Ni^{2+} =$ $Fe_2O_3(s) + =\!NiOH_2{}^+ + H^+ + H_2O$	–3.6	optimized
$Ni^{2+} + H_2O = Ni(OH)^+ + H^+$	–6.2	Ishigure et al. 1992
$Ni^{2+} + 2\,H_2O = Ni(OH)_2 + 2\,H^+$	–13.3	Ishigure et al. 1992
$Ni^{2+} + 3\,H_2O = Ni(OH)_3{}^- + 3\,H^+$	–19.7	Ishigure et al. 1992
Titration K		
$2\!\equiv\!FeOH° + Co^{2+} =$ $Fe_2O_3(s) + =\!CoOH_2{}^+ + H^+ + H_2O$	–2.5	optimized
$Co^{2+} + H_2O = Co(OH)^+ + H^+$	–6.1	Ishigure et al. 1992
$Co^{2+} + 2\,H_2O = Co(OH)_2 + 2\,H^+$	–11.7	Ishigure et al. 1992
$Co^{2+} + 3\,H_2O = Co(OH)_3{}^- + 3\,H^+$	–21.0	Ishigure et al. 1992

[†] Values from literature references interpolated at 507 K and subsequently corrected for 0.1 M using the Davies equation.

After obtaining the equilibrium constants for the adsorption reactions by fitting the titration data, we used the reaction models presented in Tables 4 and 5 to calculate the simulated pH edges shown in Figure 13. Our analysis, however, revealed that small variations in the optimized adsorption constants have a significant effect on the position

of the adsorption edges although they do not significantly impair the goodness of fit of the titration data. Hence, it would be important to supplement the titration data by taking aliquots of the suspension at various pH values and analyzing the adsorbing metal in the aqueous phase. In this study such analyses were conducted with AAS only after finishing the titrations at high pH from cooled-down and settled suspensions giving the following results: Zn 1 µM, Co 0.07 µM and Ni 0.3 µM. In all the titrations (both in the presence and absence of adsorbing metals) the iron concentration of such samples was found to be 0.3 µM.
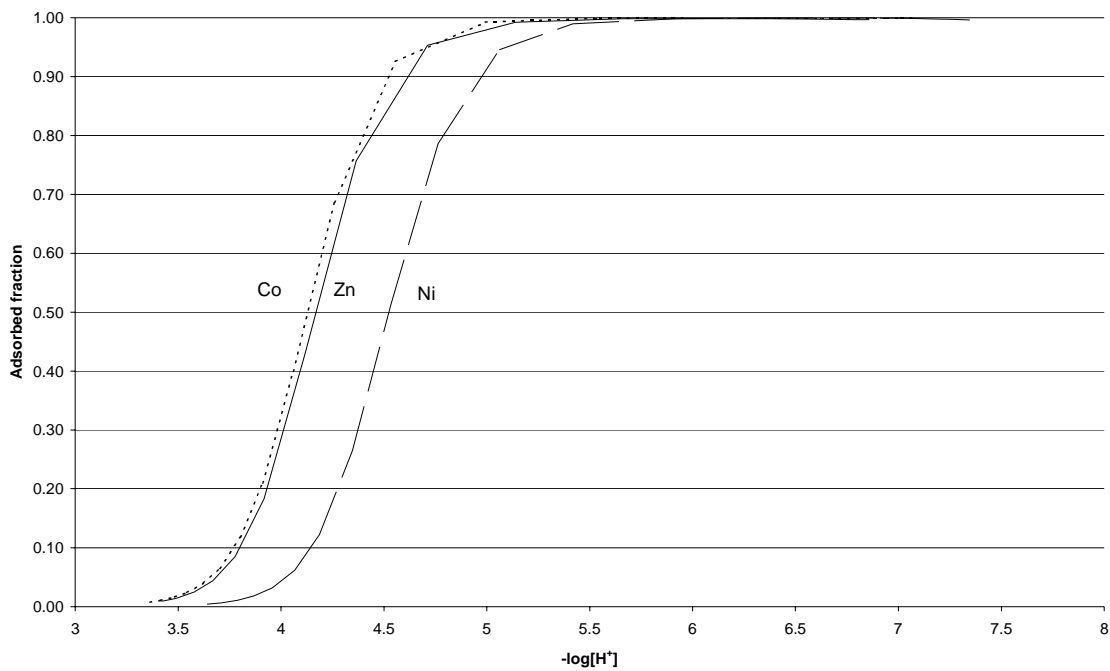

Figure 13. Adsorption of cobalt, zinc and nickel on hematite at 234 °C. Simulated tentative pH edges based on the reaction models presented in Tables 4 and 5.

3.4 Calculations on solubility and solution equilibria

The effects of heating from room temperature to high temperature were simulated by the EQ3 speciation and solubility model, and the validity of simulations was tested by the EQ6 geochemical reaction path model. EQ3 calculates a speciation of a given aqueous system and an estimation of mineral phase supersaturation. EQ6 simulates the thermodynamic state of an aqueous system during heating by starting from thermo-dynamic equilibrium and then making a small change in temperature followed by equilibration at the new temperature. The goal of this type of reaction path simulation is to quantify the chemical changes in the system during heating, including changes in pH due to both direct and indirect (e.g. variations in the solution phase composition due to changes in mineral and gas solubility) temperature effects.

The EQ3 and EQ6 input include the temperature, concentrations of elements, and the mechanism controlling the redox state of the system. The concentrations of the elements in the input can be substituted for by requiring mineral solubility equilibrium or equilibrium between the aqueous and gas phases. The required inclusion of redox equilibrium in the EQ6 simulations causes two problems in the present case. Firstly, the redox state or redox controlling mechanism during heating is not exactly known. Secondly, the program adjusts nitrogen speciation according to the calculated redox state, even in cases where such equilibrium is known not to exist due to kinetic reasons. For these reasons, most of the calculations were done by the EQ3 part of the program and the EQ6 calculations were applied as supporting information.

Some results of these simulations, which do not take into account any surface reactions, are given in Table 6. In this table, three cases in the course of the titration in the absence of any metals are considered. Case A simulates the initial acidified suspension. At room-temperature, the addition of 0.3 ml of 1 M HNO_3 to a suspension containing 10 g of hematite in 100 ml of 0.1 M $NaNO_3$ would result in a pH value of 2.6 and a total dissolved Fe concentration of 300 nM. Heating this system to 150 ^{o}C and 234 ^{o}C does not considerably change the pH, but the solubility of hematite is decreased. In cases B and C, we have simulated the titration in a similar way at neutral and alkaline regions.

Table 6. Simulated pH values and dissolved iron concentrations in the course of titrating an acidified hematite suspension with 0.1 M NaOH at three different temperatures. Case A simulates the system after acidification prior to any NaOH addition.

$T / ^{o}C$	Case A			Case B			Case C	
	pH	$[Fe]_{tot}$		pH	$[Fe]_{tot}$		pH	$[Fe]_{tot}$
25	2.64	296 nM		7.00	1.5 pM		11.4	84 pM
150	2.70	63 pM		5.82	<< 1 pM		8.95	<< 1 pM
234	2.83	1.4 pM		5.63	<< 1 pM		8.42	<< 1 pM

As a conclusion of these preliminary simulations, we can note that heating up the system does not significantly change the pH in acid conditions and hematite solubility does not seem to be a problem in our experiments. Further evidence for the latter point is given by the location of the pH break of titration curves G and L in Figure 10. The break is located close to the point where the amount of NaOH added in titration is equivalent to the amount of acid added in the initial acidification in contrast to the titration carried out in the nickel autoclave (titration D in Figure 7).

4. Conclusions and future plans

High-temperature adsorption studies are both theoretically and experimentally difficult and until now very few studies have been published. Although the values of the extracted adsorption parameters must be considered tentative, the results are encouraging, proposing the suitability of the taken approach. Although there seems to be practically no difference in the adsorption affinities between zinc and cobalt, it is easy to understand that zinc can, however, be used to retard cobalt adsorption provided that zinc concentration in the solution is considerable higher than cobalt concentration.

4.1 Surface complexation

Due to the extreme experimental conditions, uncertainties exist in the accuracy of the pH measurement and in the thermal inertness of the oxide surfaces. Special solid pretreatment procedures may be required to guarantee complete thermal inertness (insolubility and constant concentration of surface sites) of oxide surfaces in the high-temperature titrations.

Along with the readily available total proton concentration, the input data for the modelling software consist of measured free proton concentrations. The measurement is made with a pH electrode, which is a logarithmic device responding to H^+ activity. Although two procedures are available for converting the potential values measured in the extreme conditions to H^+ concentrations, there still exists some uncertainty in the obtained H^+ concentrations. Further work is needed to develop a fully reliable method for converting the measured potential values to pH or, preferably, to $-\log[H^+]$.

In addition to the pH data, it would be advantageous to obtain concentration data of the adsorbing metal in the course of the titration. This information helps to identify the number and stoichiometry of the adsorption reactions. Further, the unknown equilibrium constants can be adjusted for simultaneous best fit of the data to both the H^+ and adsorbing metal material balances. Drawing aliquots of the clear solution without significantly disturbing the adsorption equilibria requires, however, modification of the experimental setup.

Alternative approaches to the simple two-layer models for describing the electrostatic aspects of the interfacial layer are worth studying.

4.2 Molecular modelling

Until recent years, molecular modelling has been employed to a surprisingly small extent in explaining the adsorption of inorganics on oxide surfaces. As VTT Processes possesses a comprehensive expertise and extensive experience in many aspects of molecular modelling, it would be a natural extension for us to utilize the potential of molecular modelling in the study of cation adsorption on oxide films. As a first step in this direction, we present below theoretical considerations on the crystal structures of iron oxides.

For transition metal oxides, like iron oxides, one of the most typical structures is the spinel structure. The spinel name is based on the mineral, $MgAl_2O_4$, which occurs in nature (Cotton and Wilkinson 1988). Other oxides having the same arrangement of atoms in lattice structure are also called spinels. Examples of spinels are $FeAl_2O_4$, $CoAl_2O_4$, $NiAl_2O_4$, $MnAl_2O_4$ and $ZnAl_2O_4$ (Thomas and Thomas 1997). For these oxides, the general formula is $M^{II}M^{III}_2O_4$. There exist also $M^{IV}M^{II}_2O_4$ and $M^{VI}M^{I}_2O_4$ spinels.

The spinel structure is based on a cubic close-packed (*ccp*) arrays of oxide ions with cations in the tetrahedral and octahedral positions. The structure of spinels can also be symbolized as a formula $A[B_2]O_4$, where A ions are in the tetrahedral interstices, and B ions are in the octahedral interstices. These spinels are called normal spinels. An example of normal spinels is Mg_2TiO_4, the structure of which is presented in Figure 14. The unit cell of Mg_2TiO_4 contains 32 oxide ions, 16 octahedral cations and eight tetrahedral cations.
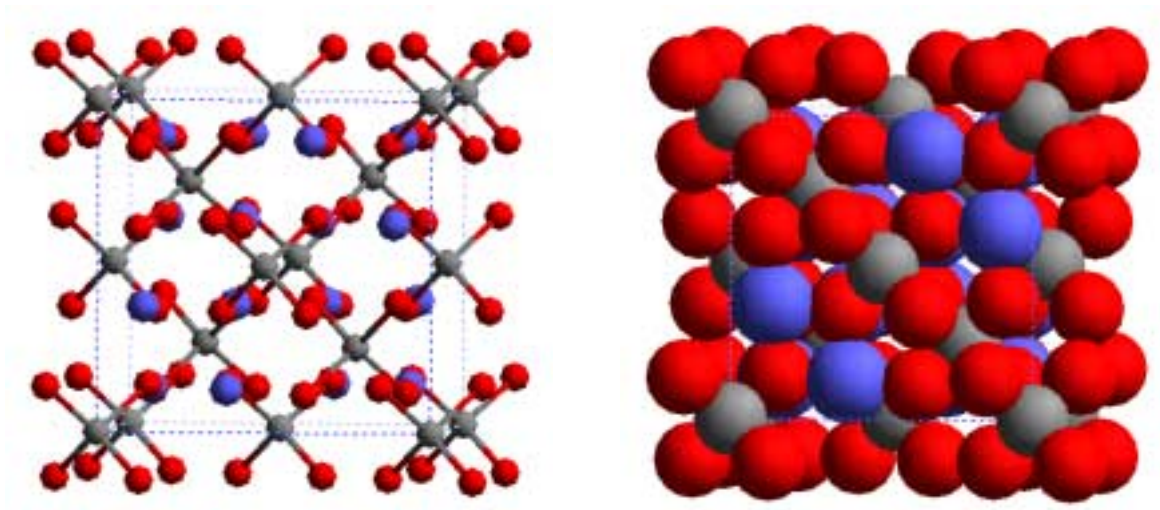

Figure 14. The crystal structure of Mg_2TiO_4 is presented by a ball and stick model (left) and van der Waals surfaces (right). Blue denotes magnesium, grey is titanium, and red is oxygen.

In order to describe the spinel structure more accurately, only the positions of cations in tetrahedral (Ti atoms) and octahedral (Mg atoms) sites are presented in Figures 15 and 16. The tetrahedral sites are located at the corners, face centers and quadrant centers in one-half of the quadrants. The octahedral sites are located in the other half of the quadrants.
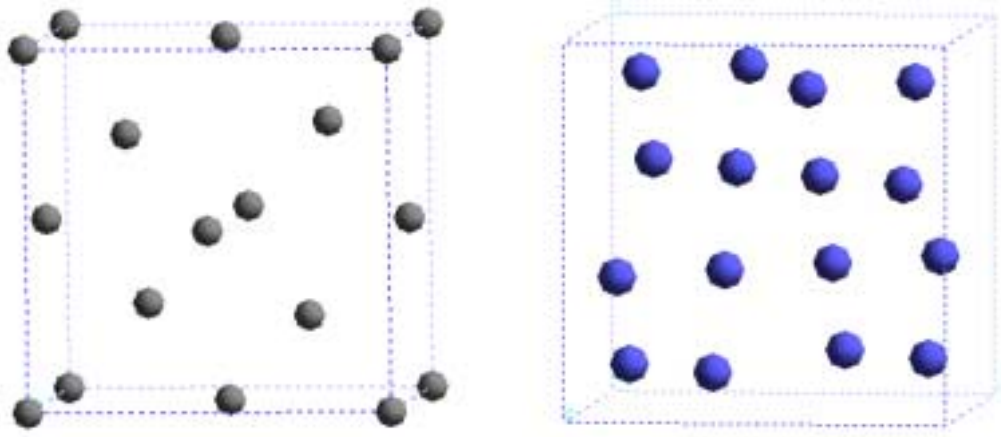

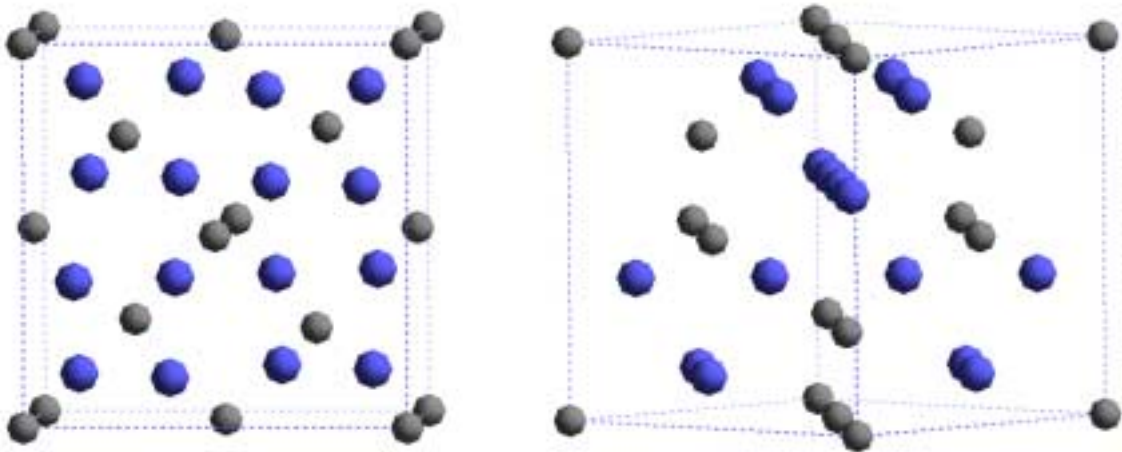*Figure 15. The positions of Ti cations (left) and Mg cations (right) in Mg_2TiO_4.*

Figure 16. The positions of Ti and Mg cations in Mg_2TiO_4 viewed from various directions. Gray denotes titanium, and blue is magnesium.

In case of the spinels, there are many structural variants. The most typical variants are inverse spinels, $B[AB]O_4$, where half of the B ions are in tetrahedral interstices, and the other half of the B ions are in octahedral interstices, together with A ions. This happens when the A ions have a stronger preference for octahedral coordination than do the B

ions. An example of inverse spinels is $Fe^{III}[Fe^{II}Fe^{III}]O_4$, where iron appears in different oxidation states (Figure 17). In order to describe the inverse spinel structure more accurately, only the positions of iron cations in the unit cell are presented in Figure 18.
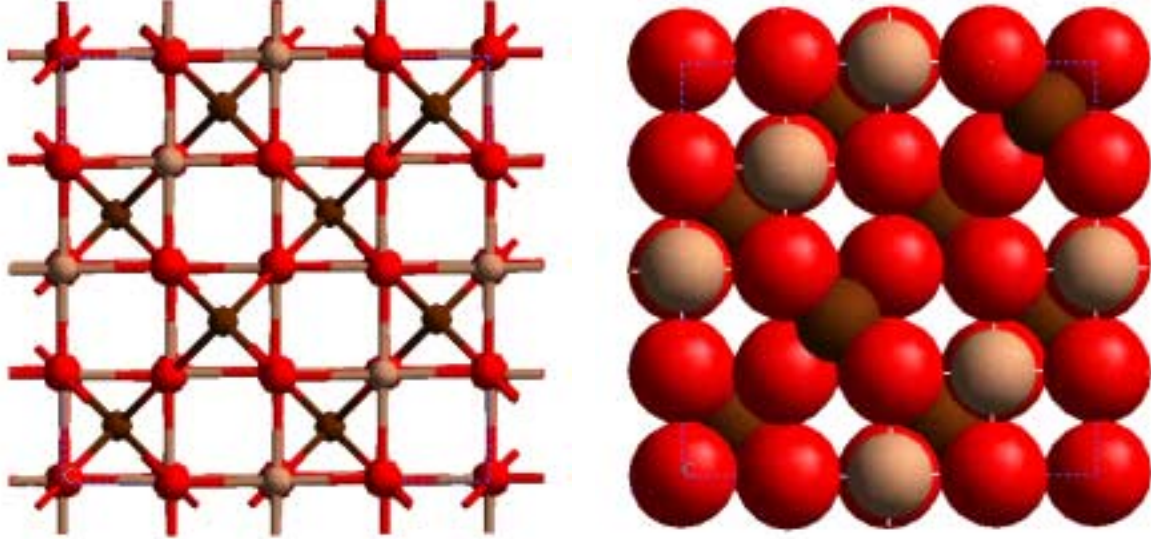

Figure 17. The crystal structure of Fe_3O_4 is presented by a ball and stick model (left) and van der Waals surfaces (right). Brown denotes iron in a tetrahedral interstice, light brown is iron in an octahedral interstice, and red is oxygen.
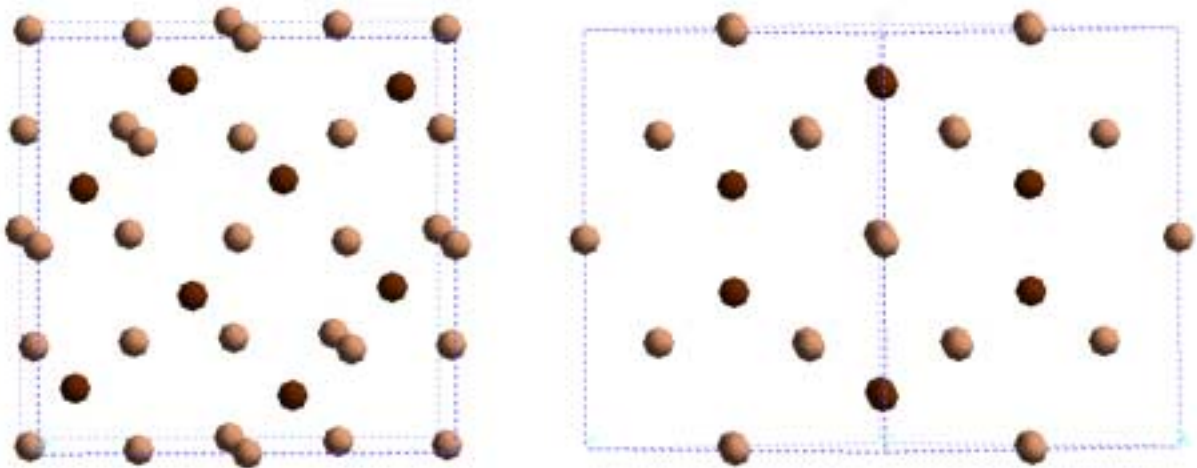
Figure 18. The positions of Fe^{II} and Fe^{III} cations in Fe_3O_4 viewed from various directions. Brown denotes iron in a tetrahedral interstice, light brown is iron in an octahedral interstice.

34

Acknowledgements

References

Baes, C. F. Jr. & Mesmer, R. E. 1976. The hydrolysis of cations. Malabar, FL: Krieger Publishing Company. 365 pp.

Bénézeth, P., Palmer, D. A., Wesolowski, D. J. & Xiao, C. 2002. New measurements of the solubility of zinc oxide from 150 to 350 °C. Journal of Solution Chemistry, Vol. 31, pp. 947–973.

Cotton, F. A. & Wilkinson, G. 1988. Advanced inorganic chemistry. New York: Wiley.

Dzombak, D. & Morel, F. 1990. Surface complexation modeling, Hydrous ferric oxide, New York: John Wiley & Sons. 393 pp.

Farley, K. J., Dzombak, D. & Morel, F. M. M. 1985. Surface precipitation model for the sorption of cations on metal oxides. Journal of Colloid and Interface Science, Vol. 106, pp. 226–242.

Fernández, D. P., Goodwin, A. R. H., Lemmon, E. W., Levelt Sengers, J. M. H. & Williams, R. C. 1997. A formulation for the static permittivity of water and steam at temperatures from 238 K to 873 K at pressures up to 1200 MPa, including derivatives and Debye-Hückel coefficients. Journal of Physical and Chemical Reference Data, Vol. 26, pp. 1125–1166.

Gran, G. 1952. Determination of the equivalence point in potentiometric titrations. Part ll. Analyst, Vol. 77, pp. 661–671.

Ishigure, K., Dinov, K., Hiroishi, D. & Matsuura, C. 1992. Solubility measurements and interactions of metal ions with oxides. Water Chemistry of Nuclear Reactor Systems 6, London: BNES, pp. 119–126.

Karasyova, O., Ivanova, L., Lakshtanov, L. & Lövgren, L. 1999. Strontium sorption on hematite at elevated temperatures. Journal of Colloid and Interface Science, Vol. 220, pp. 419–428.

Macdonald, D., Hettiarachchi, S., Song, H., Makela, K., Emerson, R. & Ben-Haim, M. 1992. Measurement of pH in subcritical and supercritical aqueous systems. Journal of Solution Chemistry, Vol. 21, pp. 849–881.

Marshall, W. & Franck, E. 1981. Ion product of water substance, 0–1000 ^{o}C, 1-10 000 bars. New international formulation and its background. Journal of Physical and Chemical Reference Data, Vol. 10, pp. 295–304.

Mäkelä, K. 2000. Development of techniques for electrochemical studies in power plant environments. Espoo: Technical Research Centre of Finland. 46 pp. + app. 128 pp. (VTT Publications 415).

Nishino, Y., Sawa, T., Ohsumi, K. & Itoh, H. 1989. Reaction rates of amorphous iron hydroxide with nickel and cobalt ions in high temperature water. Journal of Nuclear Science and Technology, Vol. 26, pp. 1121–1129.

Schoonen, M. 1994. Calculation of the point of zero charge of metal oxides between 0 °C and 350 °C. Geochimica et Cosmochimica Acta, Vol. 57, pp. 2845–2851.

Sjöberg, S., Hägglund, Y., Nordin, A. & Ingri, N. 1983. Equilibrium and structural studies of silicon (IV) and aluminium (III) in aqueous solution. V. Acidity constants of silicic acid and the ionic product of water in the medium range 0.05–2.0 M Na(Cl) at 25 ^{o}C. Marine Chemistry, Vol. 13, pp. 35–44.

Smith, R. M. & Martell, A. E. 1976. Critical stability constants, Vol. 4, Inorganic complexes. New York: Plenum Press.

Stén, P., Olin, M. & Lehikoinen, J. 2000. Surface complexation on iron oxides with reference to the oxide films formed on material surfaces in nuclear power plants. Espoo: Technical Research Centre of Finland. 70 pp. (VTT Research Notes 2055).

Thomas, J. M. & Thomas, W. J. 1997. Principles and practice of heterogeneous catalysis. Weinheim: VCH.

Wolery, T. J. 1992. EQ3/6, A software package for geochemical modeling of aqueous systems: Package overview and installation guide (Version 7.0). Livermore: Lawrence Livermore National Laboratory. 246 pp. (UCRL-MA-110662 PT I).

Author(s)

Stén, Pekka, Puhakka, Eini, Ikävalko, Ermo, Lehikoinen, Jarmo, Olin, Markus, Sirkiä, Pekka, Kinnunen, Petri & Laitinen, Timo

Title

Adsorption studies on iron oxides with reference to the oxide films formed on material surfaces in nuclear power plants

Abstract

The construction materials used in coolant systems in nuclear power plants become covered with oxide films as a result of exposure to the aqueous coolant. The present work belongs to a research program on the properties of such films and especially on the transport of inorganic species through the films. The focus is on the incorporation of the highly energetic long-lived cobalt isotope ^{60}Co in the films causing build-up of radiation fields in the out-of-core system.

The present report concentrates on experimental adsorption studies both in ambient conditions and in high-temperature (573 K and 507 K) high-pressure conditions closely resembling those prevailing in the cooling circuits of nuclear power plants. In addition to cobalt adsorption, adsorption of zinc and nickel were studied, as a novel method to decrease the activity incorporation due to ^{60}Co is injection of zinc into the primary coolant. Potentiometric acid-base titrations of hematite suspensions were conducted in the presence and absence of adsorbing metal cations (Zn^{2+}, Co^{2+}, Ni^{2+}).

Surface complexation model including surface precipitation was used to explain the high-temperature titration data. The tentative equilibrium constants of the adsorption reactions, extracted by FITEQL version 4.0 modelling software, were used to calculate high-temperature pH edges. Although there seems to be practically no difference in the high-temperature adsorption affinities between zinc and cobalt, it is easy to understand that zinc can, however, be used to retard cobalt adsorption provided that zinc concentration in the solution is considerable higher than cobalt concentration.

The construction materials used in coolant systems in nuclear power plants become covered with oxide films as a result of exposure to the aqueous coolant. The present work belongs to a research program on the properties of such films and especially on the transport of inorganic species through the films. The focus is on the incorporation of the highly energetic long-lived cobalt isotope ^{60}Co in the films causing build-up of radiation fields in the out-of-core system.

The present report concentrates on experimental adsorption studies both in ambient conditions and in high-temperature (573 K and 507 K) high-pressure conditions. Potentio-metric acid-base titrations of hematite suspensions were conducted in the presence and absence of adsorbing metal cations (Zn^{2+}, Co^{2+}, Ni^{2+}). Surface complexation model including surface precipitation was used to explain the titration data. Although there seems to be no difference in the high-temperature adsorption affinities between zinc and cobalt, it is easy to understand that zinc can, however, be used to retard cobalt adsorption provided that zinc concentration in the solution is considerable higher than cobalt concentration.